Hindawi Publishing Corporation
International Journal of Antennas and Propagation
Volume 2013, Article ID 517934, 10 pages
http://dx.doi.org/10.1155/2013/517934

Research Article

Experimental Testing of Nonredundant Near-Field to Far-Field Transformations with Spherical Scanning Using Flexible Modellings for Nonvolumetric Antennas

Francesco D'Agostino, Flaminio Ferrara, Claudio Gennarelli, Rocco Guerriero, and Massimo Migliozzi

Dipartimento di Ingegneria Industriale, Università di Salerno, Via Giovanni Paolo II 132, Salerno, 84084 Fisciano, Italy

Correspondence should be addressed to Claudio Gennarelli; gennar@diiie.unisa.it

Received 26 June 2013; Revised 24 September 2013; Accepted 4 October 2013

Academic Editor: Lorenzo Crocco

This paper deals with the experimental testing of effective probe compensated near-field-far-field (NF-FF) transformations with spherical scanning requiring a minimum number of NF data. They rely on nonredundant sampling representations of the voltage measured by the probe, based on very flexible source modellings suitable for nonvolumetric antennas characterized by two dimensions very different from the other one. In particular, a cylinder ended in two half-spheres is adopted for modelling long antennas, whereas the quasi-planar ones are considered as enclosed in a rotational surface formed by two circular "bowls" having the same aperture diameter, but eventually different bending radii. The NF data needed to perform the classical spherical NF-FF transformation are then accurately and efficiently retrieved from the acquired nonredundant ones via optimal sampling interpolation formulas. A remarkable reduction of the number of the required NF data and, as a consequence, a significant measurement time saving can be so obtained. The experimental tests have been carried out at Antenna Characterization Lab of the University of Salerno and both the NF and FF reconstructions are resulted to be very good, thus confirming the accuracy and reliability of these NF-FF transformations from the experimental viewpoint too.

1. Introduction

As is well known, most of the characteristic parameters of an antenna, as for example the radiation pattern, are defined in its far-field (FF) region. On the other hand, an accurate measurement of the electromagnetic (EM) field radiated by an antenna can be carried out only in an anechoic chamber, wherein the reflections from the walls become negligible, thus emulating the free-space propagation. However, for antennas having large or even medium electrical sizes, the FF requirements cannot be practically satisfied in an anechoic chamber, wherein only near-field (NF) measurements can be performed. Accordingly, the NF-FF transformation techniques, which allow an accurate reconstruction of the antenna far-field from measurements in the NF region, have been widely investigated and employed in the last four decades [1–9]. Among them, that employing the spherical scanning allows the complete reconstruction of the far-field without requiring the repositioning of the antenna under test (AUT). As a consequence, it has attracted a considerable attention over the years [10–22].

The classical spherical NF-FF transformation technique [16] has been modified in [17] by rigorously determining the order of the highest spherical wave to be considered and the NF data spacings on the scanning sphere taking into account the spatial band-limitation properties of radiated EM fields [23], instead of merely adopting the rule-of-thumb related to the smallest sphere able to contain the AUT. In particular, the number of data to be collected on each parallel has resulted to be decreasing when moving towards the poles. Moreover, the application of the nonredundant sampling representations of the EM fields [24, 25] has allowed a remarkable reduction of the number of needed NF data (and, as a consequence, of the measurement time) in the case of nonvolumetric antennas

characterized by one or two predominant dimensions, which have been assumed as enclosed in a prolate and oblate ellipsoid, respectively [17]. In fact, the NF data needed by the aforementioned NF-FF transformation are efficiently retrieved from the acquired nonredundant ones by means of an optimal sampling interpolation (OSI) expansion. The so-obtained measurement time saving is a very important result for the antenna measurement people because such a time is very much greater than that required for the NF-FF transformation. The hypothesis of measurements performed by an ideal probe has been removed in [18] by developing probe compensated spherical NF-FF transformations for nonvolumetric antennas. Recently, fast and accurate NF-FF transformations with spherical scanning tailored for nonspherical antennas and based on very flexible AUT modellings have been developed in [20]. In particular, a cylinder ended in two half-spheres (rounded cylinder modelling) has been employed to shape an electrically long antenna, whereas a quasi-planar one has been assumed as enclosed in a surface formed by two circular bowls (two-bowl modelling) with the same aperture diameter but with bending radii of the upper and lower arcs which can be different for fitting the actual AUT geometry better. Both the NF-FF transformations based on the ellipsoidal modellings and those using the flexible ones have resulted to be accurate and reliable as proved by the numerical simulations. Accordingly, the choice of that to be used among them depends only on the modelling which fits the shape of the considered AUT better.

At last, NF-FF transformation techniques with spherical spiral scanning, maintaining the aforementioned feature of the spherical one and exploiting continuous and synchronized movements of the positioning systems of the probe and AUT [26], have been recently proposed [27–33] to further reduce the measurement time. They rely on the nonredundant sampling representations of EM fields and employ OSI formulas to efficiently reconstruct the NF data required by the spherical NF-FF transformation from the acquired ones. In particular, the nonredundant sampling representation on the sphere from samples collected along the spiral and the related OSI expansion have been obtained in [27–29] by assuming the AUT as enclosed in the smallest sphere containing it and determining a nonredundant representation along the spiral, whose step is equal to the sample spacing needed for the interpolation along a meridian. Then, by properly applying the unified theory of spiral scans for nonspherical antennas [30], NF-FF transformations with spherical spiral scanning for electrically long or quasi-planar antennas have been developed in [31–33].

The goal of this paper is to provide the experimental validation of the nonredundant NF-FF transformations with spherical scanning for quasi-planar and electrically long antennas [20], based on the two-bowl (Figure 1) and the rounded cylinder (Figure 2) modellings, respectively. The experimental testing has been carried out in the anechoic chamber of the Antenna Characterization Lab of the University of Salerno, wherein a roll-over-azimuth spherical NF facility system is available. A very good agreement has been found both in the NF and in the FF reconstructions, thus confirming also from the experimental viewpoint the effectiveness of these nonredundant spherical NF-FF transformation techniques.

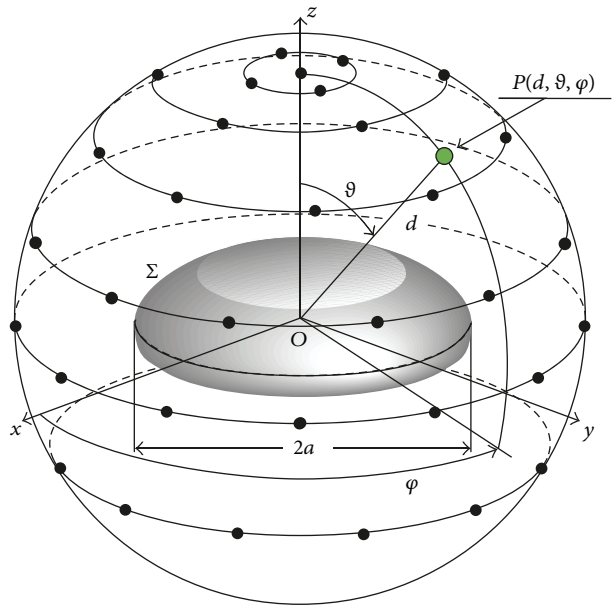

Figure 1: Spherical scanning for a quasi-planar antenna.

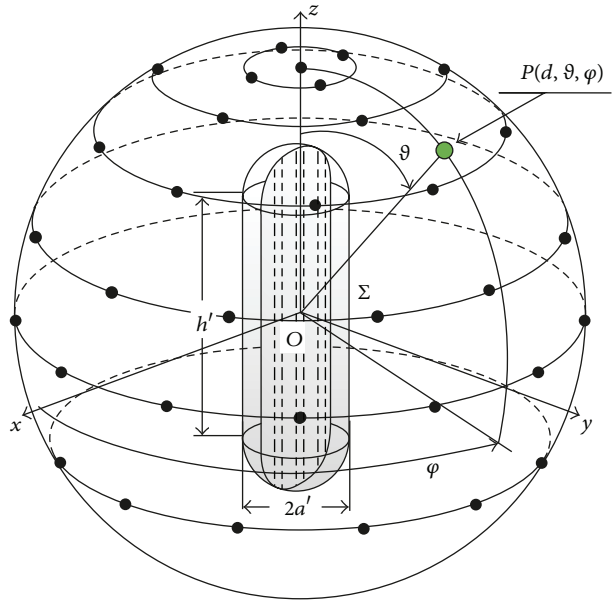

Figure 2: Spherical scanning for an elongated antenna.

2. Nonredundant Sampling Representation on a Sphere

In this section, a nonredundant and effective sampling representation [20] of the voltages V_1 and V_2, measured by the probe and rotated probe characterized by a first-order azimuthal dependence pattern on a spherical surface centered on the antenna and in its NF region, is presented. Such

a representation allows reconstructing the NF data required to perform the classical spherical NF-FF transformation, in its original version [16] or as modified in [18, 20], from the knowledge of a minimum number of samples.

Let us consider an AUT located at the origin of a spherical coordinate system (r, ϑ, φ) and a nondirective probe which scans the spherical surface of radius d (Figures 1 and 2). It has been shown [34] that the voltage V measured by such a kind of probe has the same effective spatial bandwidth of the AUT field and, accordingly, the nonredundant sampling representations of EM fields [24] can be applied to it. To this end, let us consider the AUT as enclosed in a convex domain bounded by a rotational surface Σ and introduce the "reduced voltage"

$$\widetilde{V}(\xi) = V(\xi)\, e^{j\gamma(\xi)}, \tag{1}$$

where $V(\xi)$ is the voltage V_1 or V_2, $\gamma(\xi)$ is a proper phase function to be determined, and ξ is an optimal parameter used to describe each of the curves C (meridians and parallels) representing the sphere. According to [24], the reduced voltage can be closely approximated by a band-limited function. The related band-limitation error exhibits a step-like behaviour and becomes negligible as the spatial bandwidth exceeds a critical value W_ξ [24]. Therefore, it can be effectively controlled [20] by choosing the bandwidth of the approximating function equal to $\chi' W_\xi$, where χ' is an enlargement bandwidth factor, which is slightly greater than unity for electrically large antennas.

The bandwidth W_ξ, the parameterization ξ relevant to a meridian, and the corresponding phase function γ are [20, 24]

$$\begin{aligned} W_\xi &= \frac{\beta \ell'}{2\pi}, \\ \gamma &= \frac{\beta}{2}\left[R_1 + R_2 + s_1' - s_2'\right], \\ \xi &= \frac{\pi}{\ell'}\left[R_1 - R_2 + s_1' + s_2'\right], \end{aligned} \tag{2}$$

where β is the wavenumber, ℓ' is the length of the curve C' obtained as intersection between the meridian plane through the observation point P and Σ, $R_{1,2}$ are the distances from P to the tangency points $P_{1,2}$ on C', and $s_{1,2}'$ are their curvilinear abscissae.

When considering a parallel, the phase function γ is constant and therefore it can be chosen coincident with the value relevant to the meridian through P. Moreover, it is convenient to use the angle φ as parameter. The corresponding bandwidth is given [20, 24] by

$$\begin{aligned} W_\varphi &= \frac{\beta}{2} \max_{z'} \left(R^+ - R^-\right) \\ &= \frac{\beta}{2} \max_{z'} \left(\sqrt{\left(z - z'\right)^2 + \left(\rho + \rho'(z')\right)^2} \right. \\ &\qquad \left. - \sqrt{\left(z - z'\right)^2 + \left(\rho - \rho'\left(z'\right)\right)^2} \right). \end{aligned} \tag{3}$$

In this relation, $\rho = d \sin\vartheta$, $\rho'(z')$ is the equation of Σ in cylindrical coordinates, and the maximum is attained [24] on that zone of Σ lying on the same side of the observation parallel with respect to its maximum transverse circle.

It must be stressed that, according to [24], the source modelling must fit very well the shape of the AUT in order to minimize the overall number of needed samples. As a matter of fact, the minimum number of samples at Nyquist rate required to represent the radiated EM field, and as consequence the voltage measured by a nondirective probe, on a closed observation surface enclosing the antenna is given by

$$N_\Sigma = \frac{\text{area of } \Sigma}{(\lambda/2)^2}, \tag{4}$$

with λ being the wavelength.

In light of the above considerations, when dealing with an antenna having a quasi-planar geometry, an effective and convenient modelling is obtained by choosing Σ coincident with the smallest surface formed by two circular bowls (two-bowl modelling) with the same aperture diameter but with bending radii of the upper and lower arcs eventually different to fit the actual AUT geometry better (see Figures 1 and 3). Such a modelling is very flexible. In fact, it allows a good fitting of many real antennas by properly choosing the values of the aperture diameter $2a$ and of the radii c and c' of the upper and lower arcs. For instance, the surface Σ coincides with a sphere if $c = c' = a$, it becomes a half-sphere if $c = 0$ and $c' = a$, and it reduces to a circular dish for $c = c' = 0$.

On the other hand, an effective and convenient modelling for an electrically long antenna is the rounded cylinder modelling, obtained by considering the AUT as enclosed in a cylinder of height h' ended in two half-spheres of radius a' (Figures 2 and 4).

The explicit expressions of the parameters involved in the nonredundant sampling representation using the two-bowl and the rounded cylinder modellings are reported in Appendices A and B, respectively.

In the following a two-dimensional OSI expansion, which allows the fast and accurate reconstruction of the probe voltage at any point on the scanning sphere from a minimum number of samples, is presented. Such an expansion is formally the same for both the considered AUT modellings, but the values of the parameters determining the nonredundant representation and the sampling arrangement are obviously different.

As shown in [20], the voltage at $P(\vartheta, \varphi)$ on the meridian fixed by φ can be evaluated via the OSI expansion:

$$\begin{aligned} V\left(\xi(\vartheta), \varphi\right) &= e^{-j\gamma(\xi)} \widetilde{V}\left(\xi, \varphi\right) \\ &= e^{-j\gamma(\xi)} \\ &\quad \times \sum_{m=m_0-q+1}^{m_0+q} \widetilde{V}\left(\xi_m, \varphi\right) \\ &\quad \times G\left(\xi, \xi_m, \bar{\xi}, M, M''\right), \end{aligned} \tag{5}$$

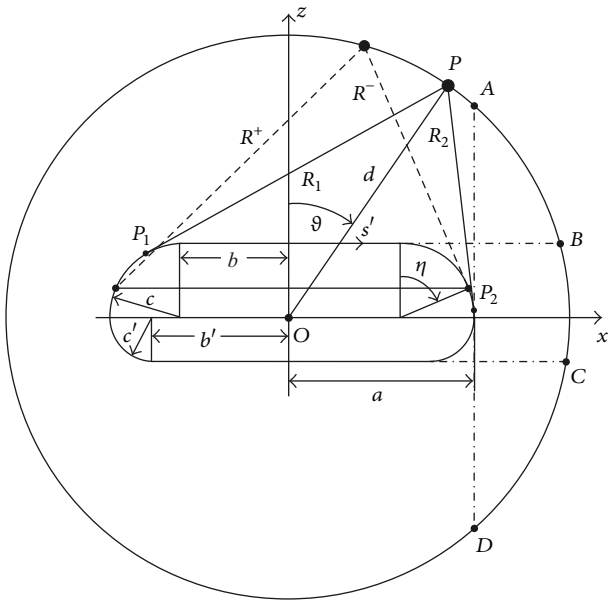

Figure 3: Relevant to the two-bowl modelling.

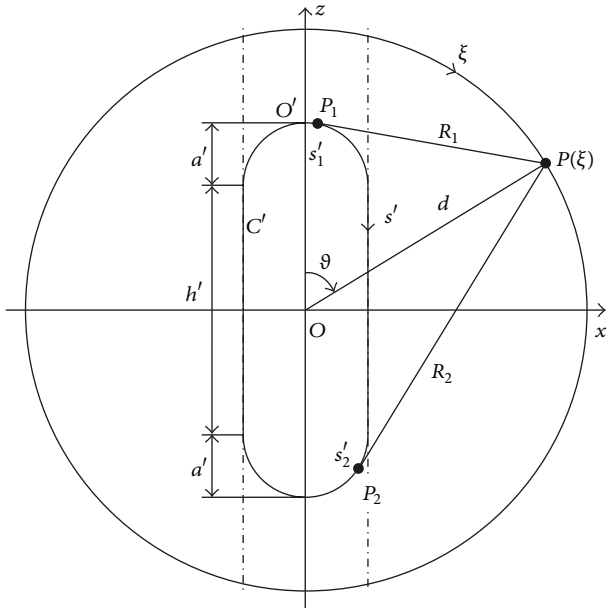

Figure 4: Relevant to the rounded cylinder modelling.

where $\widetilde{V}(\xi_m, \varphi)$ are the intermediate samples, namely, the reduced voltage values at the intersection points between the considered meridian and the sampling parallels, $m_0 = \mathrm{Int}[\xi/\Delta\xi]$ is the index of intermediate sample nearest (on the left) to P, $2q$ is the retained samples number, and

$$\begin{aligned} \xi_m &= m\Delta\xi = \frac{2\pi m}{(2M'' + 1)}, \\ M'' &= \mathrm{Int}\left(\chi M'\right) + 1, \\ M' &= \mathrm{Int}\left(\chi' W_\xi\right) + 1, \end{aligned} \tag{6}$$

with χ being an oversampling factor required to control the truncation error [35] and $\mathrm{Int}(x)$ denoting the integer part of x. Moreover,

$$G\left(\xi, \xi_m, \overline{\xi}, M, M''\right) = \Omega_M\left(\xi - \xi_m, \overline{\xi}\right) D_{M''}\left(\xi - \xi_m\right), \tag{7}$$

where

$$\begin{aligned} D_{M''}(\xi) &= \frac{\sin\left[\left(2M'' + 1\right)\xi/2\right]}{\left(2M'' + 1\right)\sin\left(\xi/2\right)}, \\ \Omega_M(\xi) &= \frac{T_M\left[2\cos^2\left(\xi/2\right)/\cos^2\left(\overline{\xi}/2\right) - 1\right]}{T_M\left[2/\cos^2\left(\overline{\xi}/2\right) - 1\right]} \end{aligned} \tag{8}$$

are the Dirichlet and Tschebyscheff sampling functions, respectively, with $T_M(\cdot)$ being the Tschebyscheff polynomial of degree $M = M'' - M'$ and $\overline{\xi} = q\Delta\xi$.

The intermediate samples can be obtained by interpolating the samples on the parallels by means of a similar OSI expansion along φ. The two-dimensional expansion for reconstructing the data at any point P on the sphere can be then determined [20] by properly matching the one-dimensional ones, thus obtaining

$$\begin{aligned} &V\left(\xi\left(\vartheta\right), \varphi\right) \\ &= e^{-j\gamma(\xi)} \sum_{m=m_0-q+1}^{m_0+q} \left\{ G\left(\xi, \xi_m, \overline{\xi}, M, M''\right) \right. \\ &\qquad \times \sum_{n=n_0-p+1}^{n_0+p} \widetilde{V}\left(\xi_m, \varphi_{n,m}\right) \\ &\qquad \left. \times G\left(\varphi, \varphi_{n,m}, \overline{\varphi}, N_m, N_m''\right) \right\}, \end{aligned} \tag{9}$$

where $\widetilde{V}(\xi_m, \varphi_{n,m})$ are the reduced samples on the parallel fixed by ξ_m, $2p$ is the retained samples number along φ, $n_0 = \mathrm{Int}(\varphi/\Delta\varphi_m)$,

$$\begin{aligned} \varphi_{n,m} &= n\Delta\varphi_m = 2\frac{\pi n}{2N_m'' + 1}, \\ N_m'' &= \mathrm{Int}\left(\chi N_m'\right) + 1, \\ N_m' &= \mathrm{Int}\left[\chi^* W_\varphi\left(\xi_m\right)\right] + 1, \\ N_m &= N_m'' - N_m', \\ \chi^* &= 1 + \left(\chi' - 1\right)\left[\sin\vartheta\left(\xi_m\right)\right]^{-2/3}, \\ \overline{\varphi} &= p\Delta\varphi_m \end{aligned} \tag{10}$$

and the other symbols have the same meanings as in (5). Note that the variation of χ^* with ξ is required to assure a band-limitation error constant with respect to ξ.

By applying the two-dimensional OSI formula (9), it is possible to accurately recover the probe and rotated probe voltages at the points required by the classical spherical NF-FF transformation in its original version [16] or as modified in [18, 20].

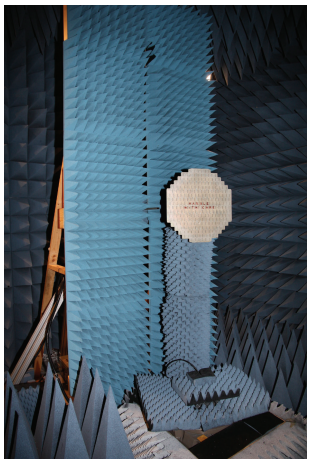

Figure 5: Photo of the spherical NF facility with the X-band flat plate slot array.

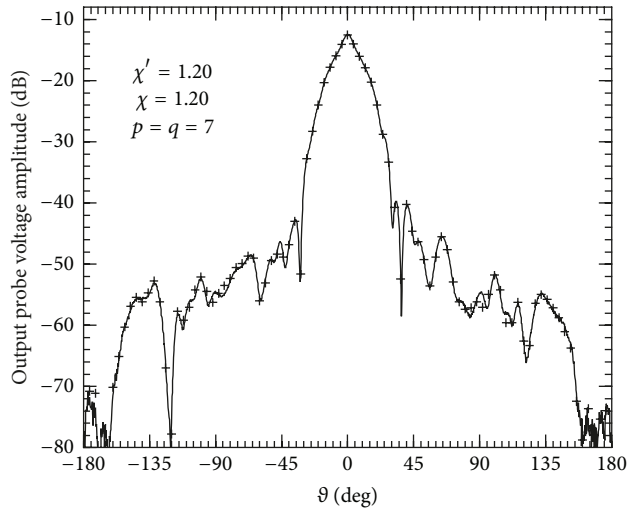

Figure 6: Amplitude of V_1 on the meridian at $\varphi = 0^\circ$. Solid line: measured. Crosses: recovered from nonredundant NF data.

3. Experimental Verification

The described nonredundant NF-FF transformations with spherical scanning for nonvolumetric antennas have been experimentally assessed in the anechoic chamber of the Antenna Characterization Lab of the University of Salerno, where a roll (φ axis) over azimuth (ϑ axis) spherical NF facility system is available (Figure 5). The chamber is 8 m × 5 m × 4 m sized and is covered with pyramidal absorbers ensuring a background noise lower than −40 dB. It is equipped with a vertical scanner and several rotating tables supplied by MI Technologies, which can be properly arranged to perform NF measurements with plane-polar, planar spiral, cylindrical, and helicoidal scannings, besides those with spherical and spherical spiral scannings. The positioning system of the AUT is mounted on two slides in order to properly set the distance from the probe to the AUT. Moreover, a further rotating table, located on the opposite side of the chamber with respect to the vertical scanner and covered by the absorbers when performing the NF measurements to avoid the decay of the anechoic chamber characteristics, allows the direct far-field measurement of small antennas as well as the radar cross section (RCS) measurements of small targets. The amplitude and phase measurements are accomplished by means of a vector network analyzer Anritsu 37247C, able to work in the frequency range from 40 MHz to 20 GHz. Both the rotating tables employed in the roll-over-azimuth spherical NF facility ensure an angular precision of ±0.05°. An open-ended WR90 rectangular waveguide scanning a sphere of radius $d = 45.2$ cm is employed as probe.

The former set of figures (from Figure 5 to Figure 11) refers to the case of a quasi-planar AUT, whereas the latter (from Figure 12 to Figure 19) is relevant to an elongated antenna.

The former antenna is an X-band flat plate slot array of Rantec Microwave Systems Inc., having a diameter of about 46 cm and operating at 9.4 GHz (see Figure 5). It is located on the plane $z = 0$ of the adopted reference system (Figure 1) and has been fitted by a two-bowl modelling with $a = 23.46$ cm,

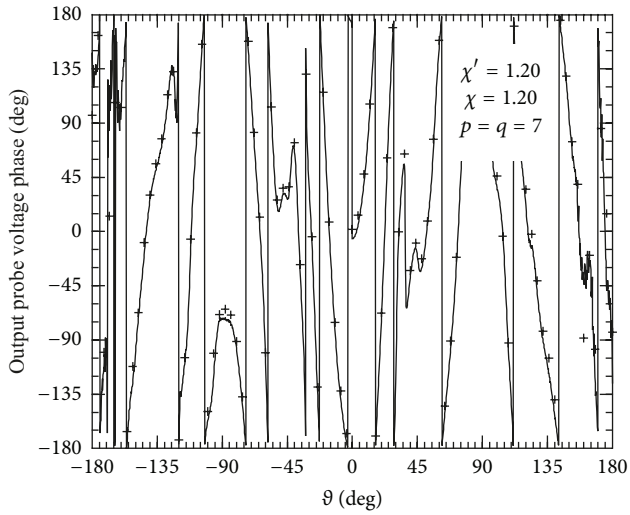

Figure 7: Phase of V_1 on the meridian at $\varphi = 0^\circ$. Solid line: measured. Crosses: recovered from nonredundant NF data.

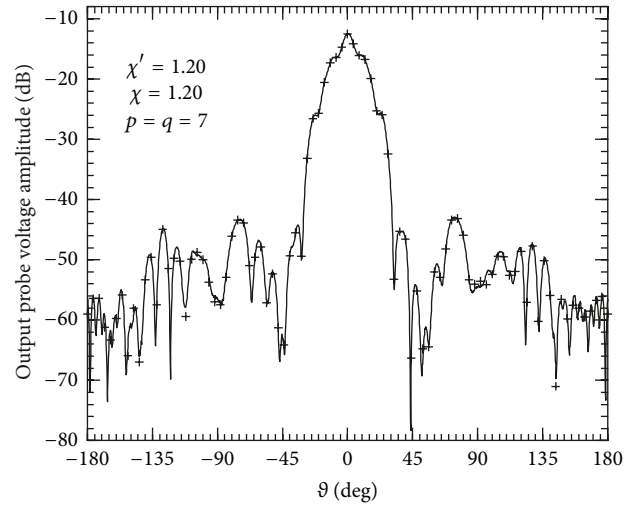

Figure 8: Amplitude of V_2 on the meridian at $\varphi = 90^\circ$. Solid line: measured. Crosses: recovered from nonredundant NF data.

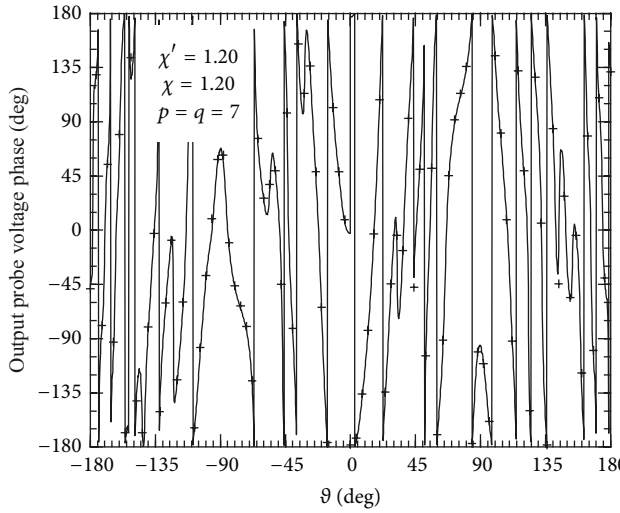

FIGURE 9: Phase of V_2 on the meridian at $\varphi = 90^\circ$. Solid line: measured. Crosses: recovered from nonredundant NF data.

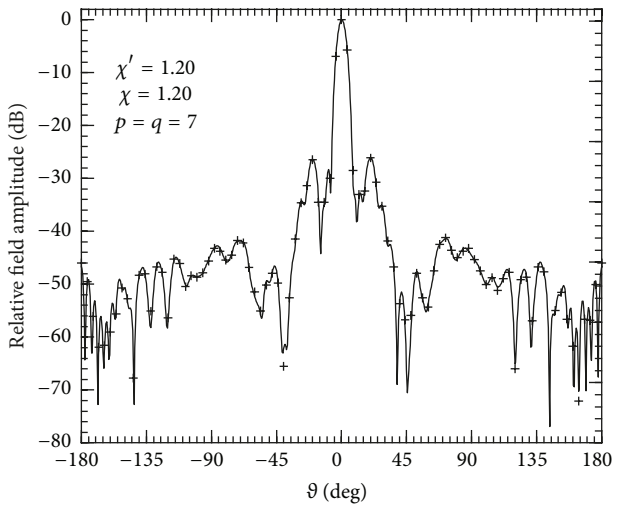

FIGURE 10: E-plane pattern. Solid line: reference. Crosses: reconstructed from nonredundant NF data.

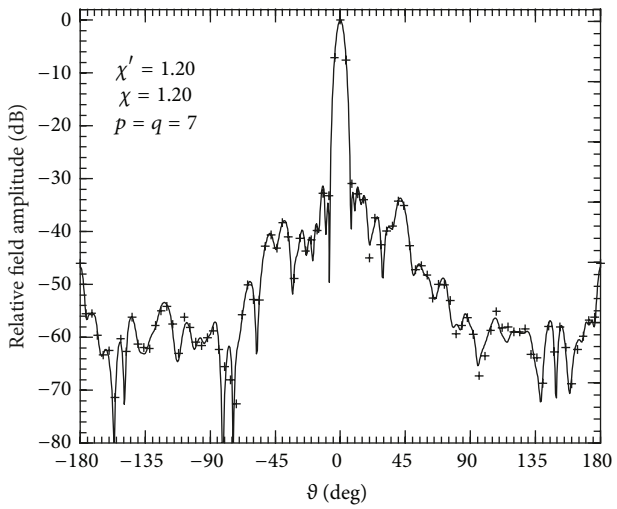

FIGURE 11: H-plane pattern. Solid line: reference. Crosses: reconstructed from nonredundant NF data.

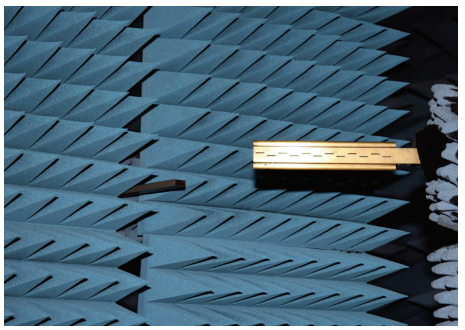

FIGURE 12: Photo of the X-band resonant slotted waveguide array.

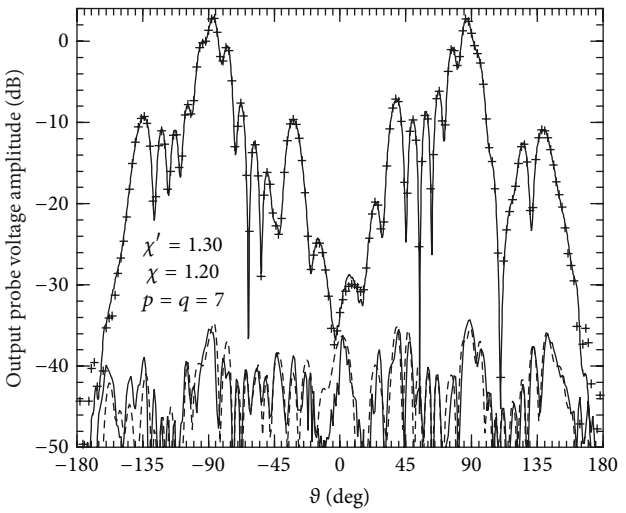

FIGURE 13: Amplitude of V_1 and V_2 on the meridian at $\varphi = 0^\circ$. Solid lines: measured. Crosses: V_1 recovered from nonredundant NF data. Dashes: V_2 recovered from nonredundant NF data.

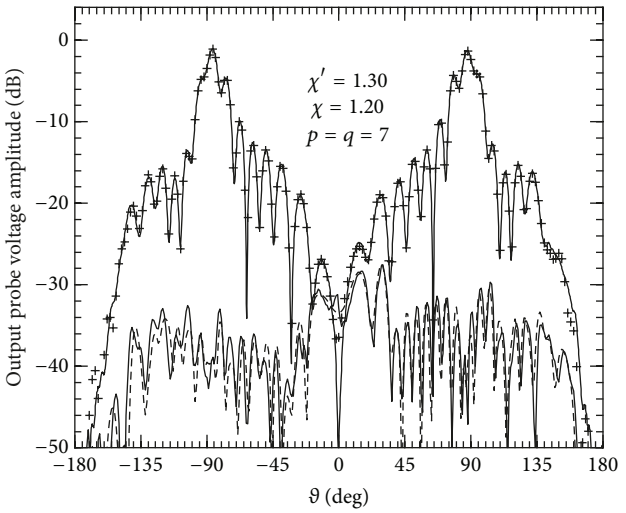

FIGURE 14: Amplitude of V_1 and V_2 on the meridian at $\varphi = 90^\circ$. Solid lines: measured. Crosses: V_1 recovered from nonredundant NF data. Dashes: V_2 recovered from nonredundant NF data.

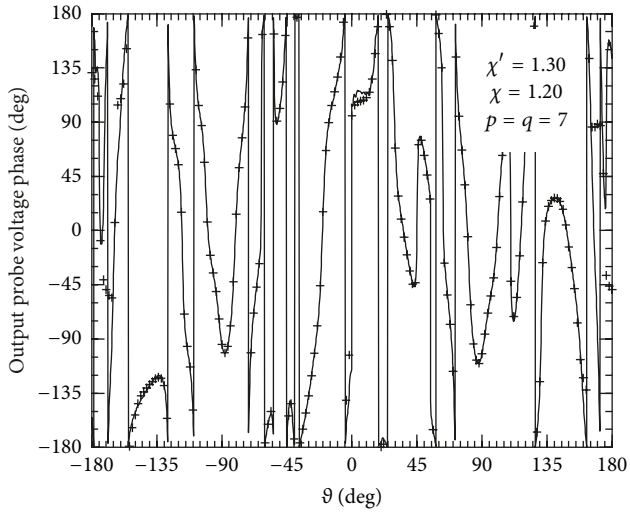

FIGURE 15: Phase of V_1 on the meridian at $\varphi = 0^\circ$. Solid line: measured. Crosses: recovered from nonredundant NF data.

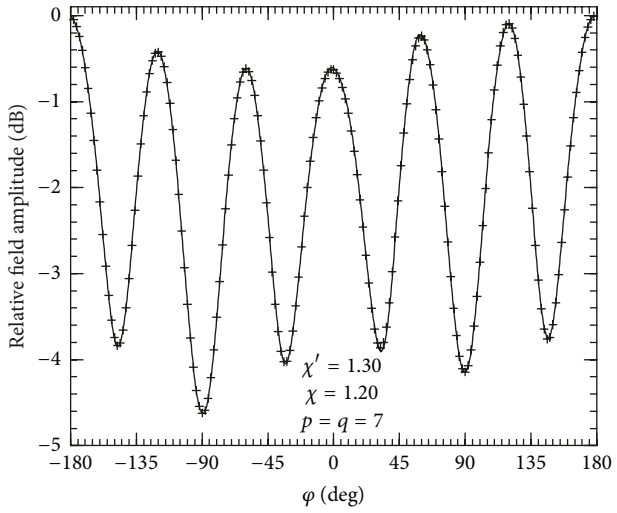

FIGURE 16: E-plane pattern. Solid line: reference. Crosses: reconstructed from nonredundant NF data.

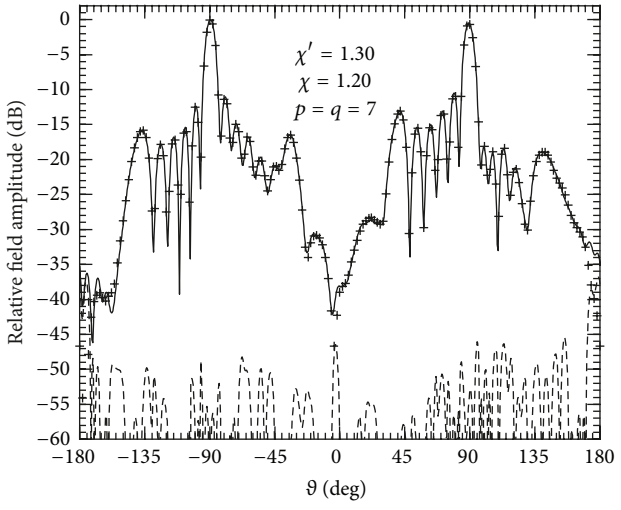

FIGURE 17: H-plane pattern. Solid line: reference. Crosses: reconstructed from nonredundant NF data. Dashed line: reconstruction error.

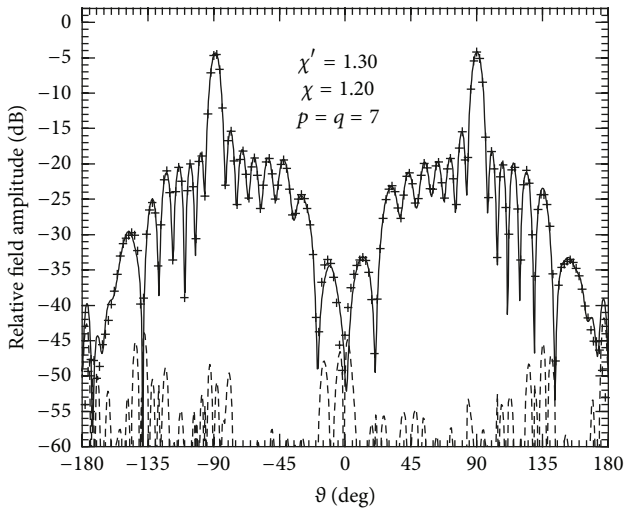

FIGURE 18: FF pattern in the cut plane at $\varphi = 90^\circ$. Solid line: reference. Crosses: reconstructed from nonredundant NF data. Dashed line: reconstruction error.

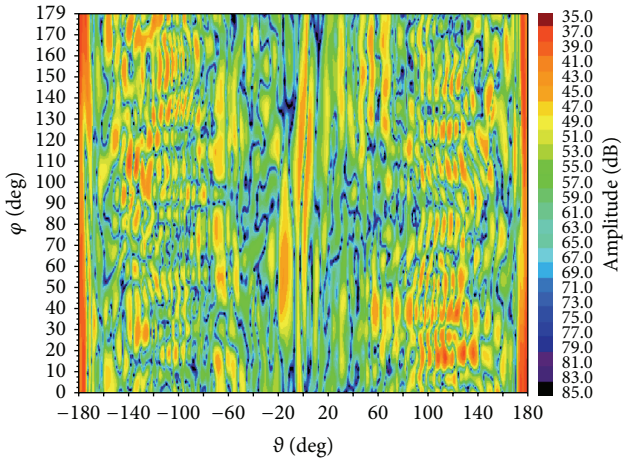

FIGURE 19: Reconstruction error over the full far-field sphere.

$c = 6.38\,\text{cm}$, and $c' = 4.79\,\text{cm}$. The reconstructions of the amplitude and phase of the voltage V_1 on the meridian at $\varphi = 0^\circ$ are shown in Figures 6 and 7, respectively, whereas those relevant to the voltage V_2 on the meridian at $\varphi = 90^\circ$ are reported in Figures 8 and 9. As can be seen, there is an excellent agreement between the recovered voltages and those directly measured, thus assessing the effectiveness of the two-dimensional OSI formula (9). As regards the values of the OSI algorithm parameters, χ' has been chosen equal to 1.20 in order to make negligible the aliasing error with respect to the measurement one [36], whereas $\chi = 1.20$ and $p = q = 7$ have been employed for neglecting the truncation error [20]. The FF patterns in the principal planes E and H reconstructed from the nonredundant spherical measurements are compared in Figures 10 and 11 with those (references) obtained from the NF data directly measured on the classical spherical grid. In both of the cases, the software package MI-3000, implementing the classical spherical NF-FF transformation [16], has been employed to get the FF reconstructions. As can

be seen, also the far-field reconstructions are very accurate, thus experimentally validating the described nonredundant spherical NF-FF transformation for quasi-planar antennas. Note that reported results have been obtained by employing (3945) NF data, significantly lower than those (7320) required by the classical NF-FF transformation [16].

The latter antenna is an X-band resonant slotted waveguide array of PROCOM, located on the plane $y = 0$ of the adopted reference system (Figure 2), working at 10.4 GHz. It has been obtained from a WR90 rectangular waveguide, by cutting 12 round-ended slots on both its broad walls, and has two cylinders soldered on its narrow walls (see Figure 12). According to the sampling representation for an elongated antenna, it has been considered as enclosed in a rounded cylinder with $h' = 28.27$ cm and $a' = 2.83$ cm. Figures 13 and 14 show the reconstruction of the amplitude of the probe voltages V_1 and V_2 on the meridians at $\varphi = 0^\circ$ and $\varphi = 90^\circ$. Moreover, the reconstruction of the phase of V_1 on the meridian at $\varphi = 0^\circ$ is reported in Figure 15. Note that, since such an AUT is characterized by a very small transverse dimension, χ' has been now chosen equal to 1.30, which ensures an aliasing error of about −40 dB, generally considered acceptable for practical purposes. As can be seen, there is a good agreement between the reconstructed voltage and that directly measured, save for the zones characterized by a very low level, wherein the error is caused by the noise and the residual reflections from the anechoic chamber walls. Obviously, better results can be achieved when increasing χ'. The overall effectiveness of the nonredundant spherical NF-FF transformation for elongated antennas is assessed by comparing in Figures 16 and 17 the reconstructed FF patterns in the principal planes with those (references) obtained from the NF data directly acquired on the classical spherical grid. Moreover, the reconstruction of the FF pattern in the cut plane at $\varphi = 90^\circ$ is shown in Figure 18. In this last figure, as well as in Figure 17, the reconstruction error is plotted also in order to better appreciate its levels. As can be seen, all reconstructions are very accurate. At last, the reconstruction error over the full far-field sphere is shown in Figure 19. It must be stressed that the employed samples are 836, whereas those needed by the MI software package, implementing the classical spherical NF-FF transformation [16], are 5100. Surely, better results can be achieved when increasing χ', but a greater number of NF data would be collected. In any case, the paper aim is to stress the NF data reduction achievable when the AUT has one or two predominant dimensions. Note that the same percentage of NF data reduction would be obtained with a significantly greater accuracy (also in the reconstruction of the cross-polarized component), if an electrically larger elongated antenna with the same ratio between the longitudinal and transverse dimensions had been considered.

4. Conclusions

An experimental validation of the nonredundant NF-FF transformations with spherical scanning for quasi-planar and elongated antennas, based on the two-bowl and rounded cylinder modellings, respectively, has been provided. The very good agreements found both in the near-field and in the far-field reconstructions confirm also from the experimental point of view the effectiveness and reliability of these transformation techniques, which allow a drastic measurement time saving retaining the accuracy of the classical spherical NF-FF transformation.

Appendices

A. Relevant to the Two-Bowl Modelling

The explicit expressions of the parameters involved in the nonredundant sampling representation using the two-bowl modelling (see Figure 3) are reported in the following.

It can be easily verified that, for such a modelling, $\ell' = 2[b + b' + (c + c')\pi/2]$, wherein $b = a - c$ and $b' = a - c'$. The expressions of the distances $R_{1,2}$ and curvilinear abscissae $s'_{1,2}$ change depending on the position of the tangency points $P_{1,2}$. In particular, five cases have to be considered when the angle ϑ covers the range $[0, \pi]$ (Figure 3).

For $0 \le \vartheta \le \vartheta_A = \sin^{-1}(a/d)$, it results in

$$R_1 = \sqrt{d^2 + b^2 + 2bd\sin\vartheta - c^2}, \qquad s'_1 = -\left(b + c\alpha_1\right), \tag{A.1}$$

$$\alpha_1 = \tan^{-1}\left(\frac{R_1}{c}\right) - \tan^{-1}\left[\frac{(b + d\sin\vartheta)}{d\cos\vartheta}\right], \tag{A.2}$$

$$R_2 = \sqrt{d^2 + b^2 - 2bd\sin\vartheta - c^2}, \qquad s'_2 = b + c\alpha_2, \tag{A.3}$$

$$\alpha_2 = \tan^{-1}\left(\frac{R_2}{c}\right) - \tan^{-1}\left[\frac{(b - d\sin\vartheta)}{d\cos\vartheta}\right]. \tag{A.4}$$

For $\vartheta_A < \vartheta \le \vartheta_B = \cos^{-1}(c/d)$, R_1, s'_1, and α_1 are again given by (A.1) and (A.2), whereas it results in

$$R_2 = \sqrt{d^2 + b'^2 - 2b'd\sin\vartheta - c'^2}, \qquad s'_2 = b + c\left(\frac{\pi}{2}\right) + c'\alpha_2, \tag{A.5}$$

$$\alpha_2 = \tan^{-1}\left(\frac{R_2}{c'}\right) - \tan^{-1}\left[d\cos\vartheta/\left(d\sin\vartheta - b'\right)\right].$$

For $\vartheta_B < \vartheta \le \vartheta_c = \pi - \cos^{-1}(c'/d)$, R_2, s'_2, and α_2 are again given by (A.5), whereas it results in

$$R_1 = \sqrt{d^2 + b^2 - 2bd\sin\vartheta - c^2}, \qquad s'_1 = b + c\left(\alpha_1 + \frac{\pi}{2}\right), \tag{A.6}$$

$$\alpha_1 = -\tan^{-1}\left(\frac{R_1}{c}\right) - \tan^{-1}\left[d\cos\vartheta/\left(d\sin\vartheta - b\right)\right].$$

For $\vartheta_C < \vartheta \le \vartheta_D = \pi - \sin^{-1}(a/d)$, R_1, s_1', and α_1 are again given by (A.6), whereas it results in

$$\begin{aligned} R_2 &= \sqrt{d^2 + b'^2 + 2b'd\sin\vartheta - c'^2}, \\ s_2' &= b + 2b' + \left(c + c'\right)\left(\frac{\pi}{2}\right) + c'\alpha_2, \\ \alpha_2 &= \tan^{-1}\left(\frac{R_2}{c'}\right) - \tan^{-1}\left[\frac{\left(d\sin\vartheta + b'\right)}{|d\cos\vartheta|}\right]. \end{aligned} \tag{A.7}$$

For $\vartheta_D < \vartheta \le \pi$, R_2, s_2', and α_2 are again given by (A.7), whereas

$$\begin{aligned} R_1 &= \sqrt{d^2 + b'^2 - 2b'd\sin\vartheta - c'^2}, \\ s_1' &= b + c\left(\frac{\pi}{2}\right) + c'\left(\frac{\pi}{2} - \alpha_1\right), \\ \alpha_1 &= \tan^{-1}\left(\frac{R_1}{c'}\right) - \tan^{-1}\left[\frac{\left(b' - d\sin\vartheta\right)}{|d\cos\vartheta|}\right]. \end{aligned} \tag{A.8}$$

As regards the determination of the maximum in (3), which allows the evaluation of the azimuthal bandwidth W_φ, it is convenient, for ϑ ranging in $[0, \pi/2]$, to introduce the angular coordinate η (see Figure 3) such that $z' = c\cos\eta$ and $\rho' = b + c\sin\eta$. It can be easily shown by means of simple geometrical considerations or analytical manipulations that this maximum is obtained in correspondence of the η value such that the derivative of $R^+ - R^-$ with respect to η is equal to zero. A similar result is obtained when $\pi/2 < \vartheta \le \pi$.

B. Relevant to the Rounded Cylinder Modelling

In this appendix, the explicit expressions of the parameters relevant to the nonredundant sampling representation based on the rounded cylinder modelling (see Figure 4) are reported.

In such a case, it results in $\ell' = 2(h' + \pi a')$. The expressions of the distances $R_{1,2}$ and arclength coordinates $s_{1,2}'$ change depending on the position of the observation point P. As shown in [20], three cases must be considered for ϑ ranging in $[0, \pi]$ (see Figure 4).

For $0 \le \vartheta \le \sin^{-1}(a'/d)$, it is obtained that

$$\begin{aligned} R_1 &= \sqrt{(d\sin\vartheta)^2 + \left(d\cos\vartheta - \frac{h'}{2}\right)^2 - a'^2}, \\ s_1' &= a'\sin^{-1}\left(\frac{a'd\sin\vartheta + R_1\left(h'/2 - d\cos\vartheta\right)}{R_1^2 + a'^2}\right), \end{aligned} \tag{B.1}$$

$$\begin{aligned} R_2 &= R_1, \\ s_2' &= a'\sin^{-1}\left(\frac{a'd\sin\vartheta - R_2\left(h'/2 - d\cos\vartheta\right)}{R_2^2 + a'^2}\right). \end{aligned} \tag{B.2}$$

For $\sin^{-1}(a'/d) < \vartheta \le \pi - \sin^{-1}(a'/d)$, R_1 and s_1' are again given by (B.1), whereas it results:

$$\begin{aligned} R_2 &= \sqrt{(d\sin\vartheta)^2 + \left(d\cos\vartheta + \frac{h'}{2}\right)^2 - a'^2}, \\ s_2' &= h' + a'\left[\pi - \sin^{-1}\left(\frac{a'd\sin\vartheta + R_2\left(h'/2 + d\cos\vartheta\right)}{R_2^2 + a'^2}\right)\right]. \end{aligned} \tag{B.3}$$

At last for $\pi - \sin^{-1}(a'/d) < \vartheta \le \pi$, R_2 and s_2' are again given by (B.3), whereas:

$$\begin{aligned} R_1 &= \sqrt{(d\sin\vartheta)^2 + \left(d\cos\vartheta + \frac{h'}{2}\right)^2 - a'^2}, \\ s_1' &= h' + a'\left[\frac{\pi}{2} - \sin^{-1}\left(\frac{R_1 d\sin\vartheta + a'\left(h'/2 + d\cos\vartheta\right)}{R_1^2 + a'^2}\right)\right]. \end{aligned} \tag{B.4}$$

For what concerns the azimuthal bandwidth W_φ, it can be shown that the maximum in (3) is reached at

$$z' = \begin{cases} z & |z| \le \dfrac{h'}{2}, \\ \left[\dfrac{h'}{2} + \dfrac{\left(|z| - h'/2\right)a'^2}{(d\sin\vartheta)^2 + \left(|z| - h'/2\right)^2}\right] & \\ \quad \times \operatorname{sgn}(z) & |z| > \dfrac{h'}{2}, \end{cases} \tag{B.5}$$

with $\operatorname{sgn}(\cdot)$ being the sign function.

References

[1] R. C. Johnson, H. A. Ecker, and J. S. Hollis, "Determination of far-field antenna patterns from near-field measurements," *Proceedings of the IEEE*, vol. 61, no. 12, pp. 1668–1694, 1973.

[2] A. D. Yaghjian, "An overview of near-field antenna measurements," *IEEE Transactions on Antennas and Propagation*, vol. 34, no. 1, pp. 30–45, 1986.

[3] J. Appel-Hansen, J. D. Dyson, E. S. Gillespie, and T. G. Hickman, "Antenna measurements," in *The Handbook of Antenna Design*, A. W. Rudge, K. Milne, A. D. Olver, and P. Knight, Eds., chapter 8, Peter Peregrinus, London, UK, 1986.

[4] E. S. Gillespie, Ed., "Special Issue on near-field scanning techniques," *IEEE Transactions on Antennas and Propagation*, vol. 36, no. 6, pp. 727–901, 1988.

[5] D. Slater, *Near-Field Antenna Measurements*, Artech House, Boston, Mass, USA, 1991.

[6] C. Gennarelli, G. Riccio, F. D'Agostino, and F. Ferrara, *Near-Field—Far-Field Transformation Techniques*, vol. 1, CUES, Salerno, Italy, 2004.

[7] M. H. Francis and R. W. Wittmann, "Near-field scanning measurements: theory and practice," in *Modern Antenna Handbook*, C. A. Balanis, Ed., chapter 19, John Wiley & Sons, Hoboken, NJ, USA, 2008.

[8] M. H. Francis, Ed., *IEEE Recommended Practice for Near-Field Antenna Measure-Ments*, IEEE Standard 1720-2012.

[9] C. Gennarelli, A. Capozzoli, L. Foged, J. Fordham, and D. J. van Rensburg, Eds., "Recent advances in near-field to far-field transformation techniques," *International Journal of Antennas and Propagation*, vol. 2012, Article ID 243203, 3 pages, 2012.

[10] F. Jensen, *Electromagnetic near-field-far-field correlations [Ph.D. dissertation]*, Technical University of Denmark, Rep. LD15, 1970.

[11] P. F. Wacker, "Non-planar near-field measurements: spherical scanning," NBSIR 75-809, Boulder, Colo, USA, 1975.

[12] F. H. Larsen, "Probe correction of spherical near-field measurements," *Electronics Letters*, vol. 13, no. 14, pp. 393–395, 1977.

[13] F. H. Larsen, *Probe-corrected spherical near-field antenna measurements [Ph.D. dissertation]*, Technical University of Denmark, Rep. LD36, 1980.

[14] A. D. Yaghjian and R. C. Wittmann, "The receiving antenna as a linear differential operator: application to spherical near-field measurements," *IEEE Transactions on Antennas and Propagation*, vol. 33, no. 11, pp. 1175–1185, 1984.

[15] J. E. Hansen and F. Jensen, "Spherical near-field scanning at the Technical University of Denmark," *IEEE Transactions on Antennas and Propagation*, vol. 36, no. 6, pp. 734–739, 1988.

[16] J. Hald, J. E. Hansen, F. Jensen, and F. H. Larsen, *Spherical Near-Field Antenna Measurements*, J.E. Hansen Ed., IEE Electromagnetic Waves Series, Peter Peregrinus, London, UK, 1998.

[17] O. M. Bucci, F. D'Agostino, C. Gennarelli, G. Riccio, and C. Savarese, "Data reduction in the NF-FF transformation technique with spherical scanning," *Journal of Electromagnetic Waves and Applications*, vol. 15, no. 6, pp. 755–775, 2001.

[18] A. Arena, F. D'Agostino, C. Gennarelli, and G. Riccio, "Probe compensated NF-FF transformation with spherical scanning from a minimum number of data," *Atti della Fondazione Giorgio Ronchi*, vol. 59, no. 3, pp. 312–326, 2004.

[19] T. Laitinen, S. Pivnenko, J. M. Nielsen, and O. Breinbjerg, "Theory and practice of the FFT/matrix inversion technique for probe-corrected spherical near-field antenna measurements with high-order probes," *IEEE Transactions on Antennas and Propagation*, vol. 58, no. 8, pp. 2623–2631, 2010.

[20] F. D'Agostino, F. Ferrara, C. Gennarelli, R. Guerriero, and M. Migliozzi, "Effective antenna modellings for NF-FF transformations with spherical scanning using the minimum number of data," *International Journal of Antennas and Propagation*, vol. 2011, Article ID 936781, 11 pages, 2011.

[21] T. B. Hansen, "Spherical near-field scanning with higher-order probes," *IEEE Transactions on Antennas and Propagation*, vol. 59, no. 11, pp. 4049–4059, 2011.

[22] T. B. Hansen, "Numerical investigation of the system-matrix method for higher-order probe correction in spherical near-field antenna measurements," *International Journal of Antennas and Propagation*, vol. 2012, Article ID 493705, 8 pages, 2012.

[23] O. M. Bucci and G. Franceschetti, "On the spatial bandwidth of scattered fields," *IEEE Transactions on Antennas and Propagation*, vol. 35, no. 12, pp. 1445–1455, 1987.

[24] O. M. Bucci, C. Gennarelli, and C. Savarese, "Representation of electromagnetic fields over arbitrary surfaces by a finite and nonredundant number of samples," *IEEE Transactions on Antennas and Propagation*, vol. 46, no. 3, pp. 351–359, 1998.

[25] O. M. Bucci and C. Gennarelli, "Application of nonredundant sampling representations of electromagnetic fields to NF-FF transformation techniques," *International Journal of Antennas and Propagation*, vol. 2012, Article ID 319856, 14 pages, 2012.

[26] R. G. Yaccarino, L. I. Williams, and Y. Rahmat-Samii, "Linear spiral sampling for the bipolar planar near-field antenna measurement technique," *IEEE Transactions on Antennas and Propagation*, vol. 44, no. 7, pp. 1049–1051, 1996.

[27] O. M. Bucci, F. D'Agostino, C. Gennarelli, G. Riccio, and C. Savarese, "Near-field-far-field transformation with spherical spiral scanning," *IEEE Antennas and Wireless Propagation Letters*, vol. 2, pp. 263–266, 2003.

[28] F. D'Agostino, C. Gennarelli, G. Riccio, and C. Savarese, "Theoretical foundations of near-field-far-field transformations with spiral scannings," *Progress in Electromagnetics Research*, vol. 61, pp. 193–214, 2006.

[29] M. Migliozzi, F. D'Agostino, F. Ferrara, J. A. Fordham, C. Gennarelli, and R. Guerriero, "An experimental validation of the near-field-far-field transformation with spherical spiral scan," *IEEE Antennas and Propagation Magazine*, vol. 55, no. 3, pp. 228–235, 2013.

[30] F. D'Agostino, F. Ferrara, C. Gennarelli, R. Guerriero, and M. Migliozzi, "The unified theory of near-field-far-field transformations with spiral scannings for nonspherical antennas," *Progress in Electromagnetics Research B*, vol. 14, pp. 449–477, 2009.

[31] F. D'Agostino, F. Ferrara, C. Gennarelli, R. Guerriero, M. Migliozzi, and G. Riccio, "A nonredundant near-field to far-field transformation with spherical spiral scanning for nonspherical antennas," *The Open Electrical & Electronic Engineering Journal*, vol. 3, no. 1, pp. 1–8, 2009.

[32] F. D'Agostino, F. Ferrara, C. Gennarelli, R. Guerriero, and M. Migliozzi, "Far-field reconstruction from a minimum number of spherical spiral data using effective antenna modelings," *Progress in Electromagnetics Research B*, vol. 37, pp. 43–58, 2012.

[33] F. D'Agostino, F. Ferrara, C. Gennarelli, R. Guerriero, and M. Migliozzi, "Experimental assessment of an effective near-field—far-field transformation with spherical spiral scanning for quasiplanar antennas," *IEEE Antennas and Wireless Propagation Letters*, vol. 12, pp. 670–673, 2013.

[34] O. M. Bucci, G. D'Elia, and M. D. Migliore, "Advanced field interpolation from plane-polar samples: experimental verification," *IEEE Transactions on Antennas and Propagation*, vol. 46, no. 2, pp. 204–210, 1998.

[35] O. M. Bucci, C. Gennarelli, and C. Savarese, "Optimal interpolation of radiated fields over a sphere," *IEEE Transactions on Antennas and Propagation*, vol. 39, no. 11, pp. 1633–1643, 1991.

[36] C. Gennarelli, G. Riccio, V. Speranza, and C. Savarese, "Fast and accurate interpolation of radiated fields over a cylinder," *Progress in Electromagnetics Research*, vol. 8, pp. 349–375, 1994.